

# Journal Pre-proof

Improving performance of perovskites solar cells using solvent engineering, via Lewis adduct of MAI-DMSO-PbI<sub>2</sub> and incorporation of imidazolium cation

Edgar González-Juárez, Diego González-Quijano, Diana F. Garcia-Gutierrez, Domingo I. Garcia-Gutierrez, Jorge Ibarra-Rodríguez, Eduardo Sanchez

PII: S0925-8388(19)34322-1

DOI: <https://doi.org/10.1016/j.jallcom.2019.153076>

Reference: JALCOM 153076

To appear in: *Journal of Alloys and Compounds*

Received Date: 7 August 2019

Revised Date: 16 November 2019

Accepted Date: 17 November 2019

Please cite this article as: E. González-Juárez, D. González-Quijano, D.F. Garcia-Gutierrez, D.I. Garcia-Gutierrez, J. Ibarra-Rodríguez, E. Sanchez, Improving performance of perovskites solar cells using solvent engineering, via Lewis adduct of MAI-DMSO-PbI<sub>2</sub> and incorporation of imidazolium cation, *Journal of Alloys and Compounds* (2019), doi: <https://doi.org/10.1016/j.jallcom.2019.153076>.

This is a PDF file of an article that has undergone enhancements after acceptance, such as the addition of a cover page and metadata, and formatting for readability, but it is not yet the definitive version of record. This version will undergo additional copyediting, typesetting and review before it is published in its final form, but we are providing this version to give early visibility of the article. Please note that, during the production process, errors may be discovered which could affect the content, and all legal disclaimers that apply to the journal pertain.

© 2019 Published by Elsevier B.V.



**Author Contributions section**

For the development of this manuscript it was necessary to form a work team in such a way that each one contributes with their experience, in this sense the authors and their contribution are listed:

Dr. Edgar González performed the MAPbI<sub>3</sub> synthesis for its application in photovoltaic devices.

Dr. Diego González conducted the first studies to obtain the ImIPbI<sub>3</sub> phase through chemical synthesis and analysis of SEM and XRD.

Dr. Domingo I. Gutierrez and Dra. Diana F. Gutierrez conducted studies of the morphology of each of the films manufactured by spin-coating and which were characterized by scanning electron microscopy (SEM).

Dr. Jorge Ibarra conducted XRD studies and Rietveld analysis

Dr. Eduardo Sánchez is the leader of the group and in addition to supporting experimentation, he is responsible for managing resources for the purchase of reagents and infrastructure.

**Improving performance of perovskites solar cells using solvent engineering, via Lewis adduct of MAI-DMSO-PbI<sub>2</sub> and incorporation of imidazolium cation.**

Edgar González-Juárez<sup>1</sup>, Diego González-Quijano<sup>2</sup>, Diana F. Garcia-Gutierrez<sup>3</sup>, Domingo I., Garcia-Gutierrez<sup>3</sup>, Jorge Ibarra-Rodríguez, Eduardo Sanchez<sup>1\*</sup>.

<sup>1</sup>Universidad Autónoma de Nuevo León, UANL, Facultad de Ciencias Químicas, FCQ, Av. Universidad S/N, Cd. Universitaria, San Nicolás de los Garza, Nuevo León, C.P. 66450, México.

<sup>2</sup>Universidad Autónoma de Aguascalientes Campus sur. Centro de Ciencias de la Ingeniería. Av. Prolongación Mahatma Ghandi 6601, Colonia el Gigante, Aguascalientes, Aguascalientes, México

<sup>3</sup>Universidad Autónoma de Nuevo León, UANL, Facultad de Ingeniería Mecánica y Eléctrica, FIME, Av. Universidad S/N, Cd. Universitaria, San Nicolás de los Garza, Nuevo León, C.P. 66450, México

## Abstract

Perovskite solar cells (PSCs) are a great promise to solve the problem of energy demand. However, one of the most important factors to obtain higher yields of high efficiency photovoltaic devices is to produce high quality methyl ammonium lead iodide (MAPbI<sub>3</sub>) films. In this work, strategies such as solvent engineering, Lewis adduction formation and the incorporation of Imidazolium cation (Im<sup>+</sup>) were implemented to improve the microstructural quality of the films. The mixed MA<sub>99</sub>ImI<sub>1</sub> film displayed a more homogeneous microstructure compared to the original MAPbI<sub>3</sub> film, as well as an improved power conversion efficiency, with a value of 17%.

*Keywords:* Perovskite solar cell, Imidazolium iodide, Thin film enhancement, solvent engineering.

## Highlights

- The quality of the film is a very important factor determining the power conversion efficiency (PCE), and it can be optimized by solvent engineering methods and incorporation of alternative MA<sup>+</sup> cations.
- ImI<sup>+</sup> has a cyclic structure of five members with two nitrogen atoms that can provide a stronger Lewis basicity to passivate sub-coordinated Pb atoms and associated defects.
- A stable 3D perovskite structure is important to improve the PCE.

## Introduction

Photovoltaic devices are one of the most promising technologies to produce electricity from sunlight. Sunlight has great potential as an alternative and renewable

energy source, with an irradiation of  $1.8 \times 10^{14}$  kW on the surface of the earth [1]. Renewable energy has a variety of sources such as solar, wind, biomass, hydraulic and geothermal [2]. Photovoltaic panels, based on silicon, show commercial efficiencies between 15-20 % [3,4] with a record efficiency of 24.4 % [5]. However, the manufacturing of these devices uses harmful chemicals and complex purification processes, as well as high cost production methodologies [6]. Recently, perovskite solar cells (PSCs) have been attracting enormous interest owing to their excellent advantages, including lower production cost, ease of fabrication, and high efficiency [7-10]; as well as unique features displayed by lead halide perovskite, such as broad and strong light absorption [11], longer charge carrier lifetime and diffusion length [12,13] and low exciton binding energy [14]. Furthermore, several research groups have achieved great success in recent years with a demonstrated power conversion efficiency (PCE) increasing rapidly from 3.8 % to 22% [15-17] in less than 5 years. However, drawbacks for a wider deployment of PSCs, despite its promising PCE, is that lead (Pb) still plays a very important role in the photovoltaic cells based on perovskites with highest efficiencies to date. Pb is known to be toxic [18,19] and efforts are ongoing to replace the Pb component of the organo-metallic halide.

However PSCs, due to its low-temperature solution processing attribute, have been fabricated on rigid or flexible substrates of small dimensions with remarkable performance, allowing greater portability, bendability, light weight, conformability, wearability and potential for integration in self powered consumer electronics, military applications for on-demand supply of electricity in missions, solar lantern, backpacks, self-powered electric cars among others.[20, 21]

Many reasons contribute to this improvement, particularly the enhanced quality of the perovskite film due to modifications on the deposition method. Various methodologies such as one-step deposition [22,23] two-step sequential deposition [24-26], solvent engineering [27], vapor-assisted deposition [28,29], additive engineering [30], and vacuum evaporation [31] can now produce high-quality films of MAPbI<sub>3</sub> with flat surfaces and complete surface coverage. Controlling the crystallization speed in the MAPbI<sub>3</sub> thin films has led to substantial improvements in the PCE of MAPbI<sub>3</sub> based PSCs. In other hand, hybrid organic-inorganic perovskites have been recently investigated for optimizing their thin films' crystal quality and to enhance the photovoltaic performance of hybrid PSCs by substitution of inorganic anions [32], metal cations [33] and organic ligands [34,35]. For instance, partially replacing methyl ammonium (MA) and formamidinium (FA) with inorganic cation Cs<sup>+</sup> [36] and Rb<sup>+</sup> [37]; replacing Pb<sup>2+</sup> with Sn<sup>2+</sup> and Ge<sup>2+</sup>; and replacing I<sup>-</sup> with Cl<sup>-</sup>, Br<sup>-</sup> [38] and SCN<sup>-</sup> [39]. Different investigations show that the size of the ionic radius (IR) of the organic cation has a great influence on the structure-property of the perovskites, which can be determined by its tolerance factor, *t*. If *t* = 1 a perfectly packed structure is expected, for *t* > 1 the perovskite tends to distort towards a tetragonal structure, finally if *t* < 1 there is a tendency to deform towards twisted octahedrons. Interestingly, perovskite cells mixed with cations such as Cs/MA [40], Cs/FA [41] and Cs/MA/FA [42] showed better stability than MAPbI<sub>3</sub>-based devices. Qian *et al.*, found that Mn<sup>2+</sup>, (IR=67 pm) doping can decrease the bandgap of CsPbIBr<sub>2</sub> and simultaneously enhance its crystallinity as well as its morphology. The PSCs constructed with CsPbIBr<sub>2</sub> reached an outstanding PCE of 7.36% [43]. Baillie *et al.* confirmed that partially replacing Pb with Ca<sup>2+</sup> (IR=100 pm) or Sr<sup>2+</sup>, (IR=118 pm) in

CsPbX<sub>3</sub> can optimize the morphology and passivate the surface states of the perovskites [44].

Imidazolium<sup>+</sup> cation (Im<sup>+</sup>) has a calculated effective radius of 258 pm [45], which is very close the calculated size of the FA<sup>+</sup> cation (253 pm), therefore it could be possible to crystallize a 3D perovskite structure with Im<sup>+</sup> replacing FA<sup>+</sup>. However, Weller [46], recently published that lead imidazolium iodide crystallizes in a 1D face-sharing infinity chains of [PbI<sub>3</sub>]<sup>-</sup> in hexagonal space group P6<sub>3</sub>/m (see Figure 1).

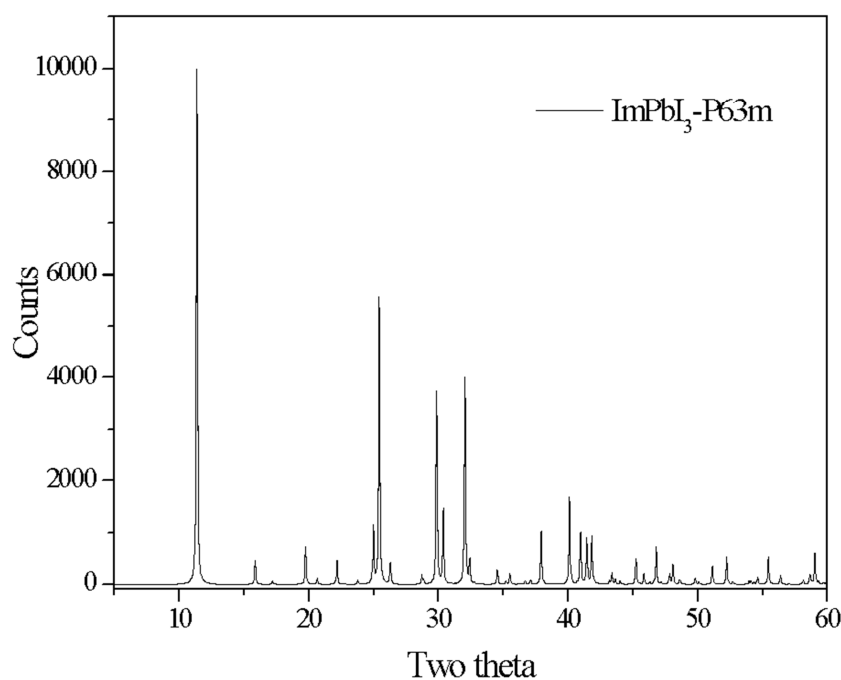


Figure 1. ImPbI<sub>3</sub> structure P6<sub>3</sub>/m

Low dimensional organo-metal halide perovskites remain relatively unfamiliar [47] and the understanding of their properties, beyond solar cells, is incomplete. Recently Jen *et al.* (2018) [48], had published on the incorporation of Im<sup>+</sup> to (MA)PbI<sub>3</sub> in an inverted perovskite solar cell configuration (NiO<sub>x</sub>/MA<sub>1-x</sub>Im<sub>x</sub>PbI<sub>3</sub>/PCBM/Bis-C<sub>60</sub>/Ag) with interesting

results, reporting a 2% increase on efficiency at 5% of  $\text{Im}^+$  incorporation. Results on further incorporation of  $\text{Im}^+$  cation into  $\text{MAPbI}_3$  on a perovskite solar cell have been recently published [49], adding an extra step in which the PSC is exposed to an atmosphere rich in methylamine. Also, an increment in the efficiency, has been related to the deprotonation of  $\text{Im}^+$  cation, which improved the quality of the thin film.

In this sense, the current work describes alternative strategies that were carried out to improve the quality of the  $\text{MAPbI}_3$  thin film using the simple mixture of  $\text{Im}^+$  and  $\text{MA}^+$  cations through solvent engineering. In the first stage, the synthesis and characterization of imidazolium iodide was carried out, using different stoichiometries. In the second stage, a cell reported in the literature was reproduced to validate the results derived from the strategies carried out to improve the quality of the  $\text{MAPbI}_3$  thin films. In the third stage chlorobenzene was used as antisolvent, and the formation of the adduct  $\text{CH}_3\text{NH}_3\text{I}-\text{PbI}_2\text{-DMSO}$  to reduce the growth rate of the crystal using a mixture of dimethylsulfoxide (DMSO) and N, N,-dimethylformamide (DMF); and finally, the incorporation of imidazolium iodide was carried out in different weight percents.

## 2. Experimental

### 2.1 Materials.

All the chemicals were used as received, including titanium diisopropoxide bis(acetylacetonate) (75 wt % in isopropanol, Sigma-Aldrich), 1-butanol (99.8%, Sigma-Aldrich), titanium oxide ( $\text{TiO}_2$ ) paste (Dyesol 18NR-T),  $\text{PbI}_2$  (99.9983%,Sigma-Aldrich), N,N-dimethylformamide (DMF, anhydrous 99.5 %, Sigma-Aldrich), lithium bis(trifluoromethylsulfonyl)imide (Li-TFSI, Sigma-Aldrich), spiro-MeOTAD (99 %, Shenzhen Feiming), chlorobenzene (SigmaAldrich), acetone, ethanol, acetonitrile.

The morphological characteristics of the thin films were observed by scanning electron microscopy (SEM) in a JEOL JCM-6000 and a Hitachi SU-8020. X-ray diffraction (XRD) was employed to characterize the crystallinity of the films using an XRD Bruker D2 phaser. The UV–Vis transmission spectra were characterized by using a scientific evolution 300 Spectrometer.

## 2.2. Perovskite standard solar cell device construction

Fluorine doped Tin Oxide (FTO) glass was patterned by chemical etching with Zinc (Zn) powder and chloride acid (HCl) solution. The etched substrate was then cleaned with hellamanex 2 % and ultrasonically cleaned with 2-propanol and deionized water in sequence for 15 min, respectively. Afterward, the substrates were further cleaned using O<sub>2</sub> plasma cleaning for 15 min. A dense layer of TiO<sub>2</sub> was then coated on the substrates by spin coating of titanium diisopropoxide bis(acetylacetonate) (75 wt% in isopropanol, Aldrich) diluted in absolute ethanol (v/v, 1/20) at 3000 rpm for 1 min. The substrates were then heated at 180 °C by 5 min followed by annealing at 450 °C for 1 h. A mesoporous layer of TiO<sub>2</sub> was then deposited by spin-coating TiO<sub>2</sub> paste (Dyesol 18NR-T) diluted in absolute ethanol at 1:12 weight ratio at 5000 rpm for 30 s. The substrates were then heated at 180 °C for 5 min, followed by annealing at 450 °C for 1h. For the fabrication of the standard cell, the methodology proposed by Sutanto *et al.*, 2017 [50], was followed, using DMF as solvent. Previously prepared solution 1.25 M of PbI<sub>2</sub>: MAI with a 1: 1 molar ratio and left at 70° C for 12 h. MAPbI<sub>3</sub> solution was deposited by spin-coating on the mesoporous layer of TiO<sub>2</sub> at 5000 rpm for 30 s. After 4 s of having started the centrifugation technique, 400 µL of chlorobenzene were rapidly added to the substrate. Furthermore, a hole transport material (HTM) of Spiro-OMeTAD was spin-coated at 3000 r.p.m. for 30 s from a chlorobenzene solution (79.1 mg in 690

$\mu\text{L}$ .) that contained 22  $\mu\text{L}$  of 4-tert-butylpyridine and 15  $\mu\text{L}$  of Li-TFSI (Bis(trifluoromethane)sulfonimide lithium salt ) from a 500 mg/ml stock solution in acetonitrile as dopants.

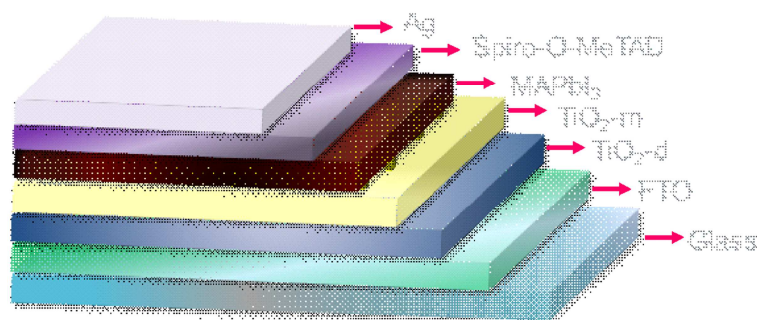


Figure 2. Configuration of the standard cell based on perovskite

To study the effect of  $\text{Im}^{+1}$  on  $\text{MAPbI}_3$  on the performance of the photovoltaic device,  $\text{Im}^{+1}$  was incorporated in a different stoichiometric ratio. The perovskite film was deposited also by spin coating a previously prepared solution 1.15 M of  $\text{MAI}:\text{PbI}_2$  with a 1:1 molar relation in a solvent mixture of DMF/DMSO (80:20 v/v) by a one-step process at 3000 r.p.m. for 30 s. After a 6 s delay time of the spin coating process, a 650  $\mu\text{L}$  of anhydrous chlorobenzene were added on top of the substrate. Additionally, perovskite thin films were sintered at 100  $^\circ\text{C}$  for 10 min. HTM was spin coated at 3000 rpm for 30 s. Finally, an 80 nm thick silver counter electrode was deposited under high vacuum by physical vapor deposition.

### 2.3. Photovoltaic characterization

The J-V curves were measured using a solar simulator (Newport, Oriel Instruments, 91160A) with a source meter (Keithley 2400). In addition, a Xenon lamp was used as a light source and the illumination source was calibrated using a silicon reference solar cell (enlitech) to calibrate the output power of the lamp to 1000 W/m<sup>2</sup>. The measurements were performed inside the glove box in order to protect the stability of the cells. The cell area was limited using a metal mask (2.54mm x 2.54mm). The active area of device is 0.65 mm<sup>2</sup>.

## 2.4 Synthesis of Imidazolium iodide

Initially a purification of the HI (Iodhydric acid) solution was carried out; a 0.36 M solution of tributyl phosphate in chloroform was prepared, and a liquid-liquid extraction was carried out in a separating funnel. For crystallization, 10 ml of HI solution was used, and 0.9412 g of imidazole was dissolved, the mixture was poured into a crystallizer and slow evaporation was prevented. The iodine crystals were recrystallized with ethanol and anhydrous diethyl ether.

## 3.0 Results and Discussion

### 3.1 Characterization of hybrid compounds; Imidazolium iodide and Pbl<sub>2</sub>

In a first stage, the synthesis of the perovskite type ImPbl<sub>3</sub> was carried out by means of the ImI and Pbl<sub>2</sub> precursors to be evaluated in the active layer of the photovoltaic cell. The precursors were heated at 120° C for two hours and characterized by SEM, FT-IR, UV-Vis. Furthermore, the stoichiometry of the hybrid system ImI-Pbl<sub>2</sub> was varied, 1:1 and 2:1. The absorption spectra in solution are shown in figure 3a, where two absorption peaks are observed, located in  $\lambda_{\max}=268$  and 354 nm, these

absorption peaks are attributed to the energy transitions of  $n-\pi^*$  and  $\pi-\pi^*$ , respectively. FT-IR analysis of the hybrid system was carried out. Figure 3b shows the FTIR spectra acquired. In general, the same bands are observed in both spectra, since in both systems the same functional groups are present, the difference in intensity was related to the stoichiometry (Table 1).

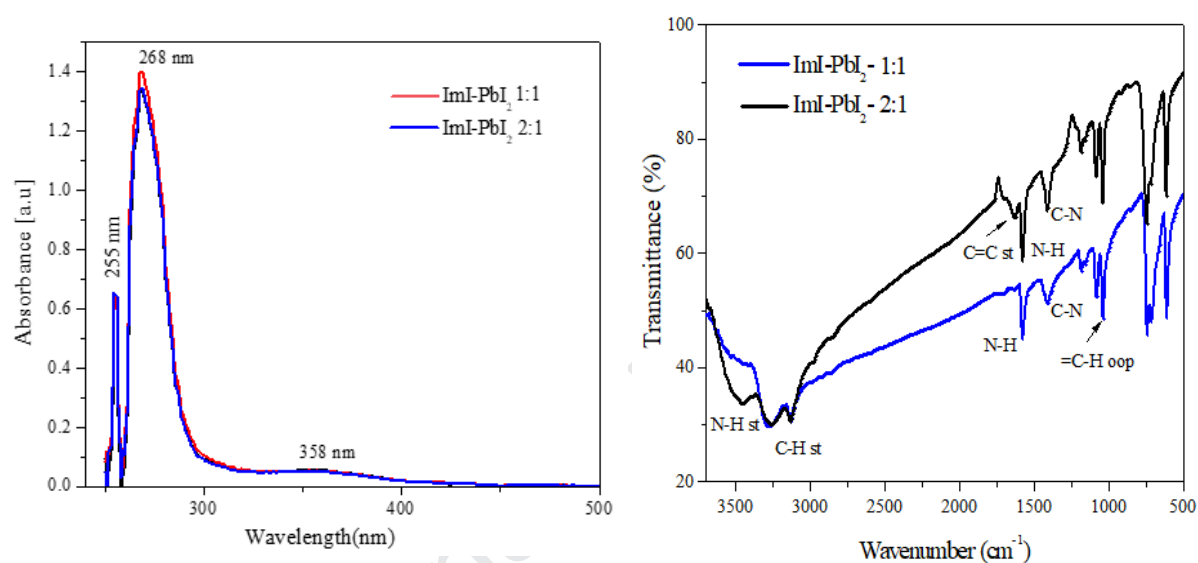


Figure 3. Characterization of the hybrid ImI-PbI<sub>2</sub> systems. 3a) Absorption; 3b) spectrum FT-IR.

X-ray diffraction analysis initially shows the absence of precursor materials, indicating the formation of another phase for both systems. ImPbI<sub>3</sub>-P6<sub>3</sub>/m was used as reference and it is observed that the hybrid 1:1 system synthesized shows the same pattern of peaks at 11.3°, 25.2°, 27°, 30.5°, 31.95°, 37.88° and 40°. However, studies of single crystals of Imidazolium iodide show that the peak that appears in 11.3° corresponds to the plane (110) of a one-dimensional structural arrangement [51-53]. This one-dimensional arrangement is attributed to the size of the ImI<sup>+1</sup> cation that does

not allow the formation of a stable 3D structure, despite complying with the Goldsmith law previously mentioned.

On the other hand, the hybrid system 2:1 shows a different pattern, with peaks at  $42.6^\circ$ ,  $21.4^\circ$ , and the  $11.3^\circ$  peak can still be observed. This suggests that the excess of Imidazolium iodide generates the combination of different phases, indicating the necessity to perform more thorough studies in order to confirm it.

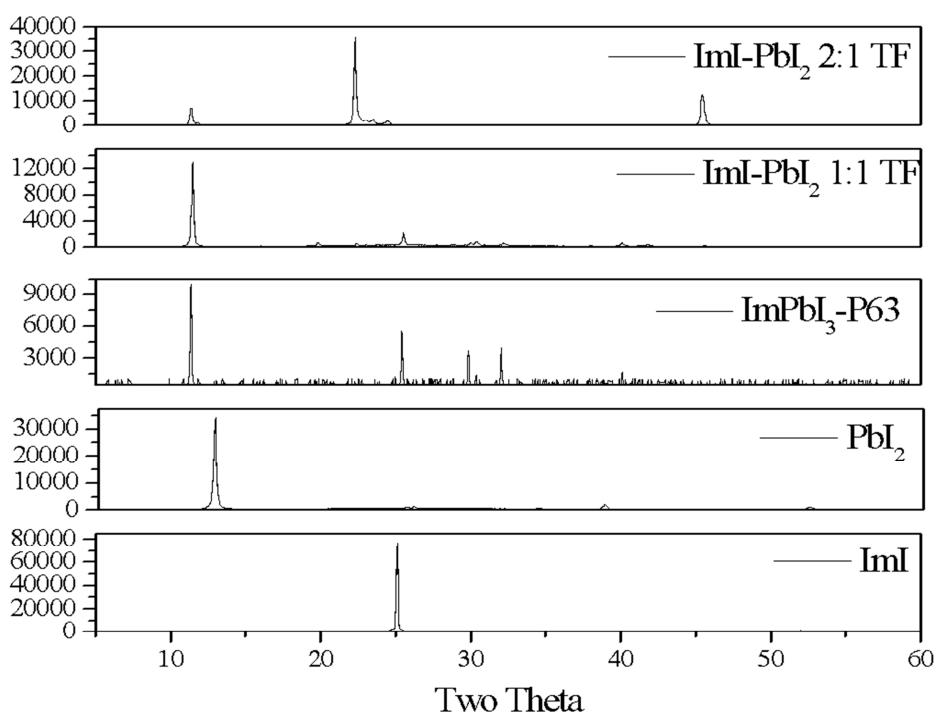


Figure 4. XRD patterns of precursors, pattern and hybrid system 1:1 and 2:1

Moreover, films were prepared for both systems by mixing the Imidazolium iodide and PbI<sub>2</sub> in DMF and heated at 90 ° C for 2 h. The solutions were deposited by spin-coating with a centrifuge ramp at different times with a heat treatment of 120 ° C for 1 h.

The films manufactured were pale yellow and in general both systems show irregularities that limit their application in photovoltaic devices. SEM images of the fabricated thin films are shown in figure 5. The hybrid system (2:1) shows the formation of agglomerates due to the excess of imidazolium, while the film of the system (1:1) shows many spaces that generate a non-homogeneous morphology. Clearly, the quality of the films offers an opportunity to perform optimization through solvent engineering that has recently been implemented for the optimization of thin film quality.

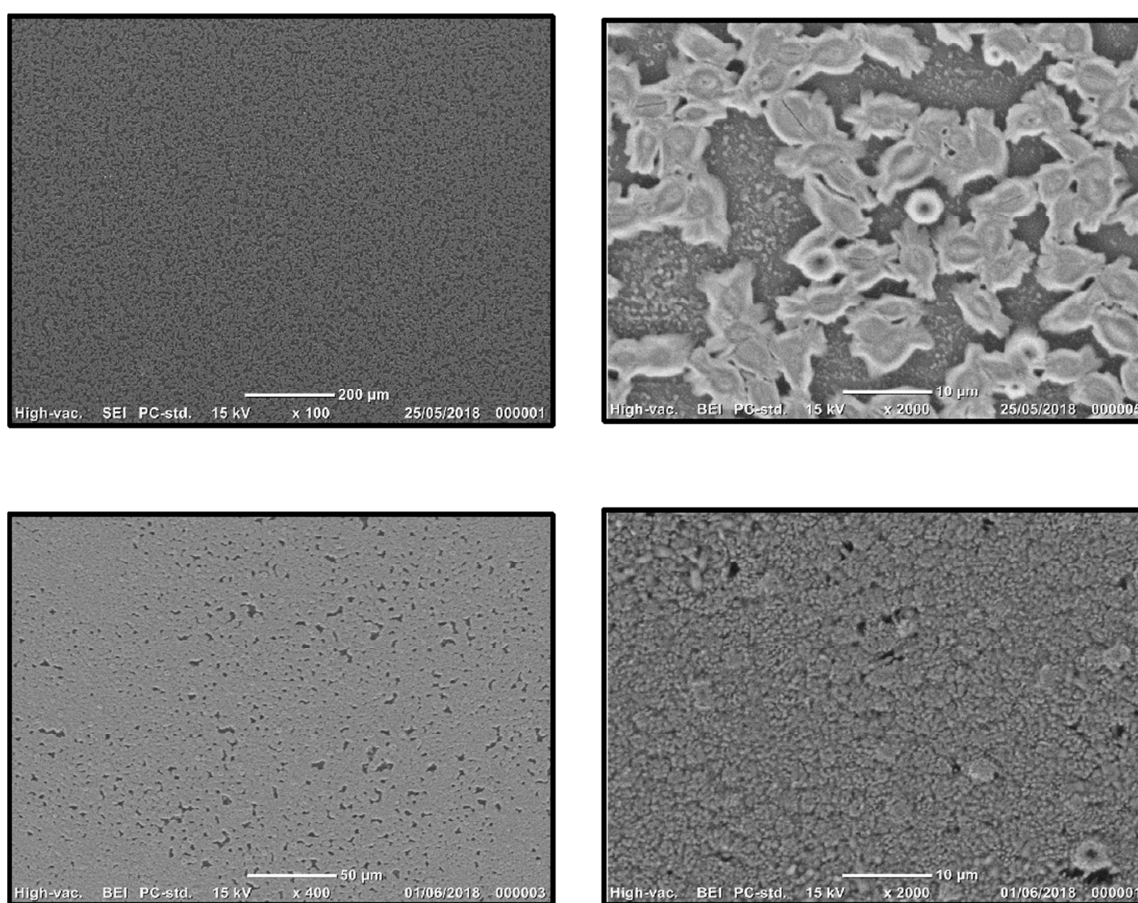


Figure 5. SEM Micrographics the hybrid system 1:1 and 2:1.

### 3.2 Optimization and performance of standard perovskite solar cell

The manufacture of the devices by this methodology produced solar cells with PCE of approximately 16% (Figure 6a). However, problems associated with the humidity of one of the precursors, in this case MAI, produced that the films that were subsequently manufactured became opaque and resulted in a significant drop in the photovoltaic performance, down to a PCE of approximately 5 % (figure 6b).

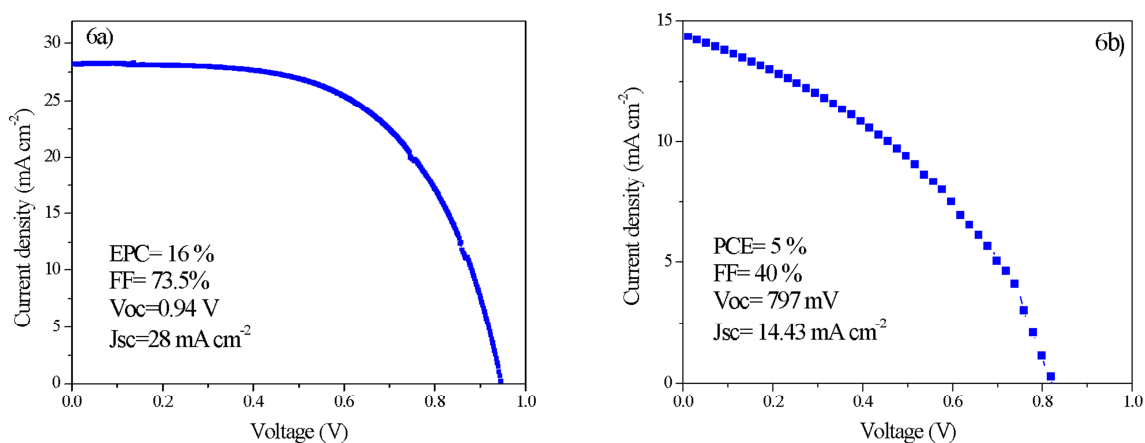


Figure 6. Current voltage (J-V); a) Standard cell; b) Cell with wet precursor (MAI)

MAI was recrystallized using ethanol and diethyl ether as solvents, left in a vacuum oven at 0.5 atm at 60° C overnight. On the other hand, it has been reported that PbI<sub>2</sub> contains a certain percentage of humidity, and in this sense, it was also put in the oven for drying. Despite the treatment given to both precursors, the MAPbI<sub>3</sub> films again became opaque. In order to improve the quality of MAPbI<sub>3</sub> films, the methodology proposed by Yinhke *et. al.*, 2017 [54] was followed, modifying both the MAPbI<sub>3</sub> concentration from 1.25 M to 1.15 M and other parameters. A mixture of DMF / DMSO solvents (80:20) was used to dissolve the precursors at 65°C for 45 minutes. The

purpose of using this mixture of solvents is to control the rapid nucleation and the rate of crystallization to optimize the morphology of the films.

Obtained MAPbI<sub>3</sub> thin films displayed an improved quality, this may be attributed to the formation of adducts between DMF and DMSO with the precursors, specifically MAI-PbI<sub>2</sub>-DMF and MAI-PbI<sub>2</sub>-DMSO [55]. Although the mechanisms of formation of these adducts have not been fully studied, their interaction with the anti-solvent (chlorobenzene) improves the quality of the MAPbI<sub>3</sub> thin films in two respects: (1) washed away the excess solvent, which is harmful for high-quality film formation; (2) promoted the formation of intermediate phases, and thus retarded the crystallization of MAI and PbI<sub>2</sub> [54]. Subsequently, the solution was deposited on the substrate chlorobenzene as antisolvent. The use of chlorobenzene or toluene during the spin coating process generates a dense and uniform layer of MAPbI<sub>3</sub> [54]. Afterward, MAPbI<sub>3</sub> films were subjected to a heat treatment to remove the volatile DMSO from the adduct. A post annealing process is always indispensable to achieve good crystallinity. In the early research of perovskite solar cells, simple annealing processes at 70–100 °C for 10– 45 min were often employed to achieve an adequate PCE for the resulting devices. Although the PCE of 16 % was not achieved, it was improved significantly from 5 % to 13%.

### **3.3 Integration of imidazolium cations into the structure of the MAPbI<sub>3</sub>**

The next stage included the incorporation of imidazolium iodide within the structure of the perovskite. Imidazolium iodide was incorporated in different percentages by weight in order to analyze the effect on the structure-property of the perovskite, its effect on photovoltaic performance and stability. Four different percentages were prepared

(MA:Iml; 0.95:0.5, 99:1, 97:3, 95:5) and labeled as follows  $MA_{0.95}Iml_{0.5}Pbl_3$ ,  $MA_{99}Iml_1$ ,  $MA_{97}Iml_3$ ,  $MA_{95}Iml_5$ ). As control, a film of pure  $MAPbl_3$  was prepared as well. The manufacturing of the devices is described in section 2.2 and the J-V curves showing their performance are displayed in figure 7, and Table 2 shows the photovoltaics parameters.

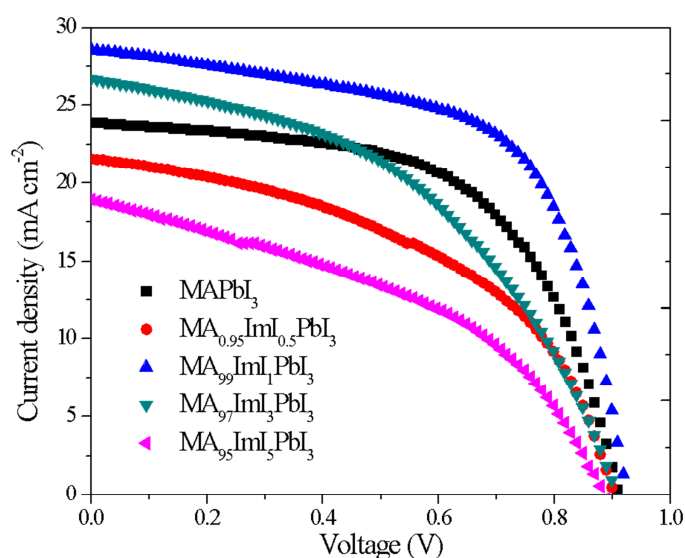


Figure 7. Figure. J-V curves of the best efficiencies obtained in this study.

Table 2. Photovoltaic parameters for a batch of 18 cells for each mixture and a standard deviation of 1.1 on average.

Perovskite	Jsc [ $mA\ cm^{-2}$ ]	Voc [V]	FF	$\eta$ [%]
$MAPbl_3$	23.90	0.91	58.4	13
$MA_{99.5}Iml_{0.5}Pbl_3$	21.57	0.90	47.6	9
$MA_{99}Iml_1Pbl_3$	29.33	0.93	63.6	17
$MA_{97}Iml_3Pbl_3$	26.7	0.90	46.1	11
$MA_{95}Iml_5Pbl_3$	18.92	0.88	42.6	7

XRD results for the MAImPbI<sub>3</sub> systems are shown in figure 8. The diffractograms show the same peaks of greater intensity at 14 °, 28 ° and 31.7 °, corresponding to the planes (110), (220) and (310), respectively (figure 8a); these peaks correspond to those previously reported by Jen *et. al.* [48] for an inverted cell; ITO /NiO<sub>x</sub> / MA<sub>1-x</sub>I<sub>x</sub>PbI<sub>3</sub> / [6,6]-phenyl-C<sub>61</sub>-butyric acid methyl (PCBM) / bis-C<sub>60</sub>/Ag. In this study a correlation was found between the efficiency of the photovoltaic device and the presence of PbI<sub>2</sub>, indicated by peak at approximately 12.55° for each of the mixtures (figure 8b). In this sense, the diffractograms of MA<sub>95</sub>I<sub>5</sub>PbI<sub>3</sub> and MA<sub>95.5</sub>I<sub>0.5</sub>PbI<sub>3</sub> show a more intense peak at ~12.55°, associated to the presence of PbI<sub>2</sub>. It is well known that the presence of PbI<sub>2</sub> significantly affects the photovoltaic performance for this type of devices. The efficiencies achieved using these compositions were 9% and 7%, respectively. On the other hand, in the MA<sub>99</sub>I<sub>1</sub>PbI<sub>3</sub> and MA<sub>97</sub>I<sub>3</sub>PbI<sub>3</sub> mixtures, this peak shows a lower intensity, and consequently these samples displayed higher efficiencies of 17% and 11%, respectively.

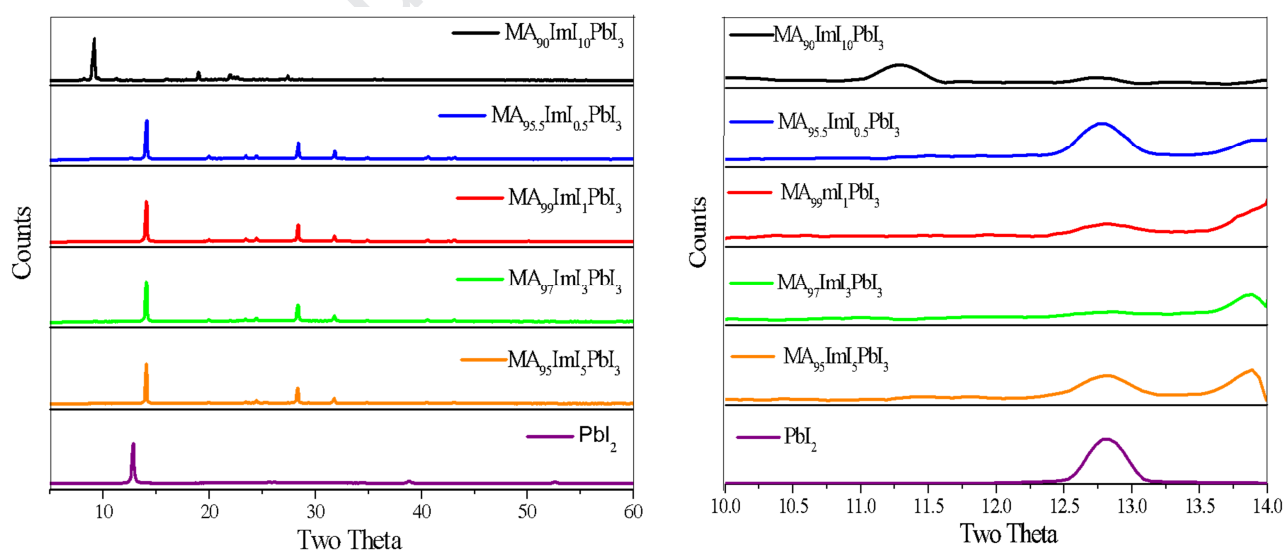


Figure 8a. XRD patterns of MA<sub>1-x</sub>I<sub>x</sub>PbI<sub>3</sub> films; 8b) highlighted diffraction profiles in the range from 2θ 10°-14°

In the analysis by SEM (figure 9) very similar microstructures can be observed. These differences are associated with the Marangoni effect, discussed by Sautanto *et. al.* [50], they explain that the roughness of the perovskite film results from the mass transfer of two solvents, the sudden turbulence of a second injection causes, to a large extent, liquid-solid phase separations and non-homogeneous concentrations to form gradient differences of tension on the perovskite surface before evaporation of the solvents. The surface tension gradient causes a random crystallization of the perovskite and a rougher surface is obtained. In general,  $\text{MAPbI}_3$ ,  $\text{MA}_{95.5}\text{ImI}_{0.5}\text{PbI}_3$ ,  $\text{MA}_{97}\text{ImI}_3\text{PbI}_3$ ,  $\text{MA}_{95}\text{ImI}_5\text{PbI}_3$  present a random crystallization, that is, a greater roughness that influences the efficiencies, whereas  $\text{MA}_{99}\text{ImI}_1\text{PbI}_3$  shows a more homogenous morphology and resulted in a higher efficiency of 17 %. It is important to highlight the absence of pinhole on the surface the film. This is attributed to the incorporation of  $\text{ImI}^{+1}$  that has a cyclic structure of five members with two N atoms that can provide a stronger Lewis basicity to passivate sub-coordinated Pb atoms and associated defects. In addition, it can form hydrogen bonds with iodide atoms at two different angles, which can form a molecular block at the grain boundaries to harden the  $\text{MAPbI}_3$  domains and improve overall robustness and device performance [48].

a)

b)

c)

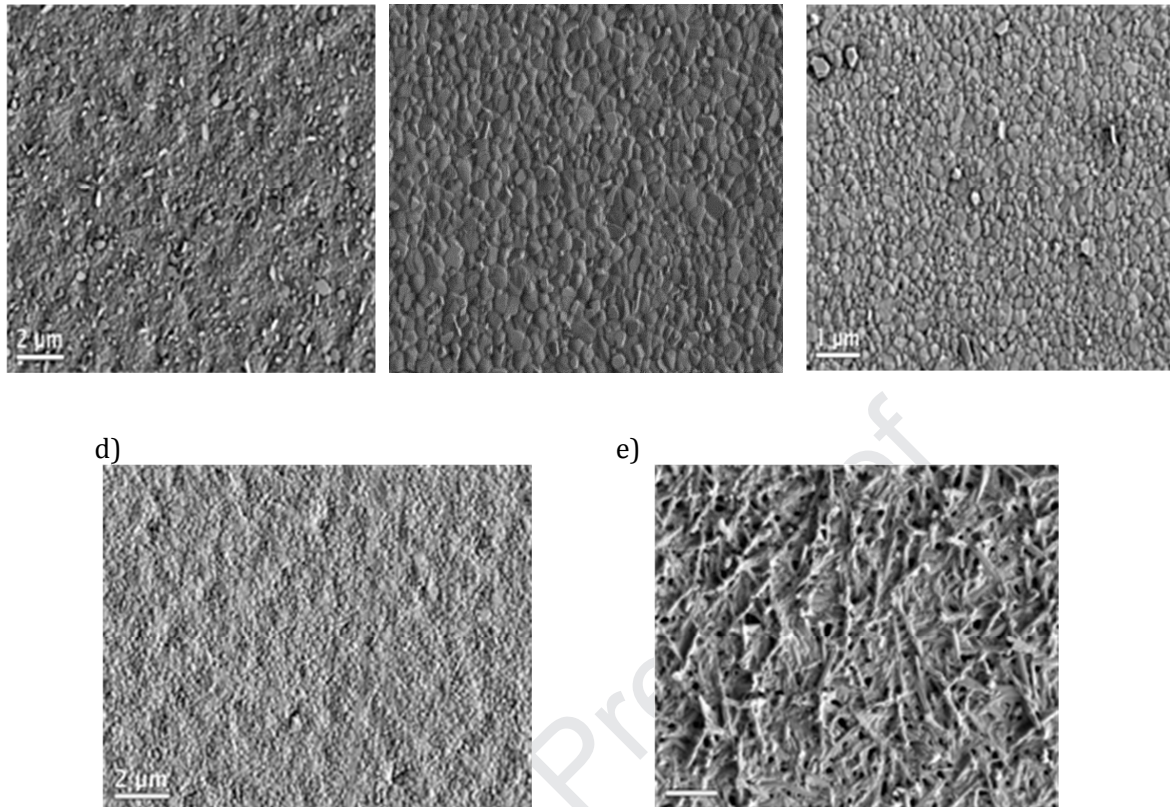


Figure 9. Scanning Electron Microscopy (SEM) images for the  $\text{MAPbI}_3$  perovskite layers; a)  $\text{MAPbI}_3$ , b)  $\text{MA}_{95.5}\text{Iml}_{0.5}\text{PbI}_3$ , c)  $\text{MA}_{99}\text{Iml}_1\text{PbI}_3$ , d)  $\text{MA}_{97}\text{Iml}_3\text{PbI}_3$ , e)  $\text{MA}_{95}\text{Iml}_5\text{PbI}_3$

It has been studied that the under-coordinated iodides in perovskite thin-films tend to act as hole-trapping sites to create charge accumulation and cause undesirable charge recombination. These defects can be passivated by the incorporation of systems that behave as bases of Lewis such as thiophene, pyridine [56].

On the other hand, it is well-known that perovskite films tend to degrade into other chemical species in humid environments, due to the reaction of perovskite materials with water in air. Other factors found are thermal effects, ultraviolet radiation and processing solutions. Different studies have suggested that water is the catalyst for the irreversible

degradation reaction of perovskite and its degradation mechanism has also been extensively studied.

In this study, moisture stability of the as-prepared perovskite films was tested under approximately 50 % RH (relative humidity) in ambient conditions without any encapsulation. In this sense, the diffractograms show a significant increase of the characteristic peak of  $\text{PbI}_2$  at  $12.5^\circ$  as the time of exposure to humidity increases. This same behavior was presented by the other systems (figure 10).

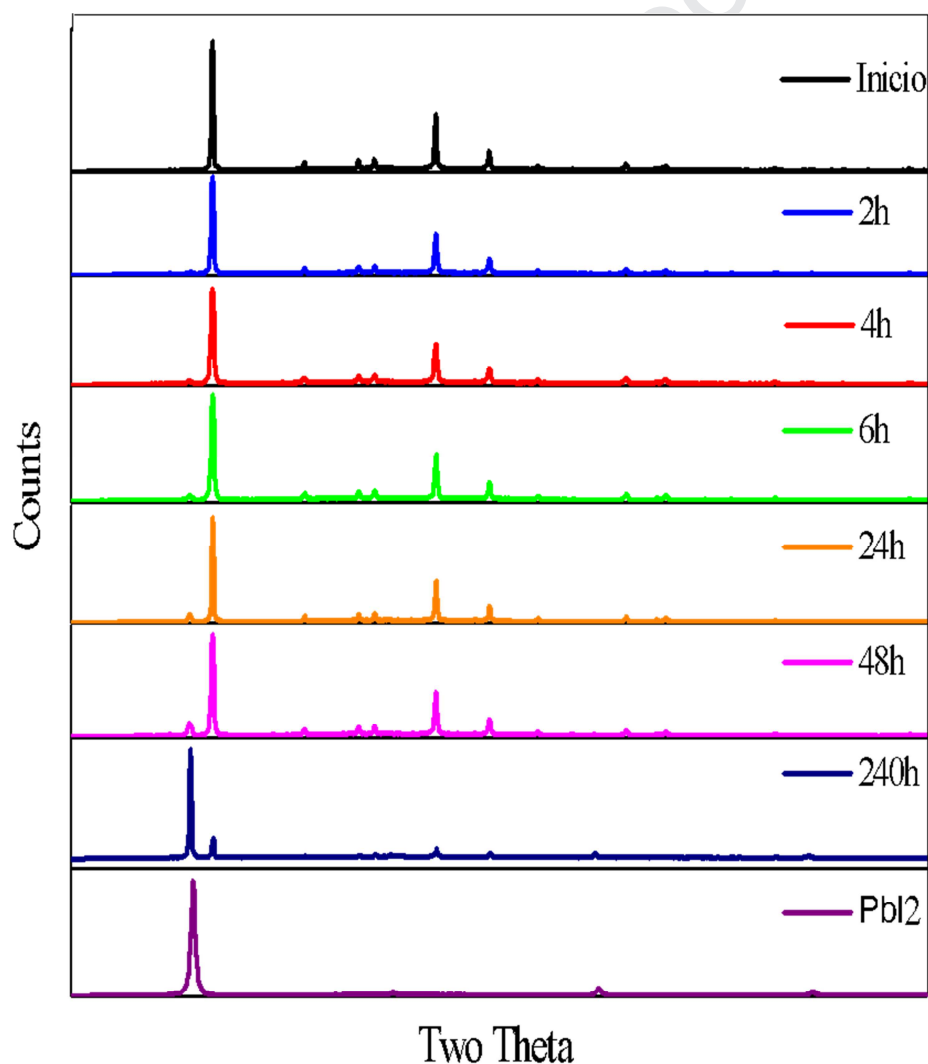


Figure 10. XRD patterns of stability of  $\text{MA}_{1-x}\text{IA}_x\text{PbI}_3$

At the same time a stability analysis was carried out for the manufactured cells. The results show that during the first 8 h there is a gradual loss of efficiency, however, after 48 h they begin to suffer the effect of humidity that is reflected in the decrease in the performance of the photovoltaic devices.  $\text{MA}_{99}\text{ImI}_1\text{PbI}_3$  film showed greater stability during this time retaining 59 % of its initial PCE, attributed to a better crystallinity, since the grain boundaries of the film retard the diffusion of moisture and oxygen. On the other hand,  $\text{MAPbI}_3$ ,  $\text{MA}_{95.5}\text{ImI}_{0.5}\text{PbI}_3$ ,  $\text{MA}_{97}\text{ImI}_3\text{PbI}_3$  and  $\text{MA}_{95}\text{ImI}_5\text{PbI}_3$  could only retain 15%, 22%, 18% and 12.5%, respectively.

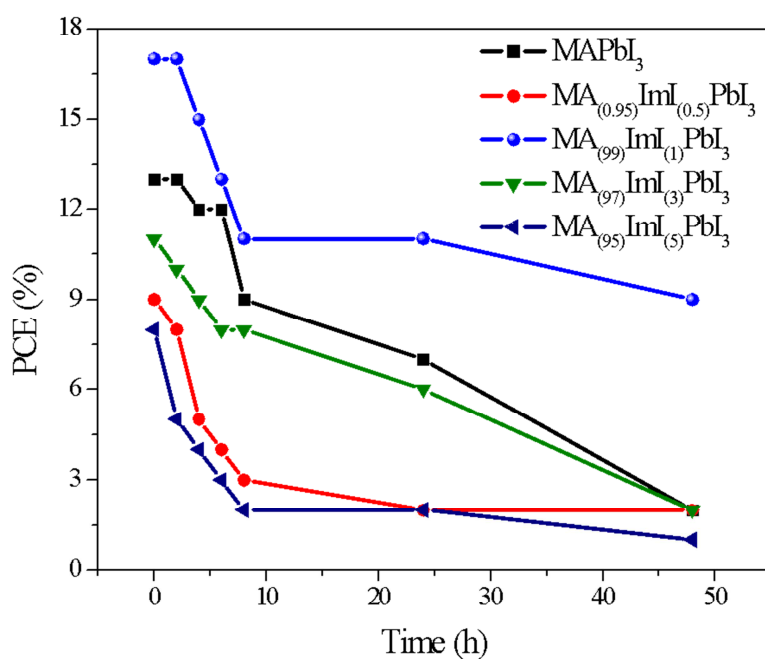


Figure 11.  $\text{MA}_{1-x}\text{IA}_x\text{PbI}_3$  PCE vs degradation time

#### 4. Conclusions

The films  $\text{ImIPbI}_3$  were pale yellow and the analysis by XRD revealed a 1-dimensional structure(1D), so its use in photovoltaic devices is limited-

Different strategies were explored to optimize the  $\text{MAPbI}_3$  film and its photovoltaic performance. Solvent engineering favored the formation of good film quality by increasing the conversion efficiency from 5 to 13%.

A method of site-A engineering was used to improve the quality of the perovskite film. The incorporation of  $\text{ImI}^+$  favored the photovoltaic performance observing different morphologies. The best PCE obtained was 17%, through the combination of  $\text{MA}_{99}\text{ImI}_1\text{PbI}_3$ , with  $V_{oc}= 0.93\text{V}$  and  $J_{sc}=29.33 \text{ mA cm}^{-2}$ . At the same time, it presented greater stability, attributed to better crystallinity, since the grain boundaries of the film retard the diffusion of moisture and oxygen.

#### 5.0 References

- [1] Panwar NL, Kaushik SC, Kothari S, Role of renewable energy sources in environmental protection: a review, *Renew Sustain Energy Rev* 2011;15(3):1513.
- [2] BP Statistical Review of World Energy 2017; 2017. Available from: (<https://www.bp.com/content/dam/bp/en/corporate/pdf/energy-economics/statistical-review-2017/bp-statistical-review-of-world-energy-2017-full-report.pdf>).
- [3] SunPower; 2017. ([www.us.sunpower.com](http://www.us.sunpower.com)).
- [4] Fraunhofer – photovoltaics report; 2017. Available from: (<https://www.ise.fraunhofer.de/content/dam/ise/de/documents/publications/studies/Photovoltaics-Report.pdf>).
- [5] Green MA, Hishikawa Y, Warta W, Dunlop ED, Levi DH, Hohl-Ebinger J, et al. Solar cell efficiency tables (version 50). *Progress Photovolt: Res Appl* 2017;25(7):668–76.

- [6] Mulvaney D. Hazardous materials used in silicon PV cell production: a primer. *Sol Ind* 2013.
- [7] H. Zhou, Q. Chen, G. Li, S. Luo, T. Song, H. Duan, Z. Hong, J. You, Y. Liu, Y. Yang, Interface engineering of highly efficient perovskite solar cells, *Science* 345 (2014) 542–546. <https://doi.org/10.1126/science.1254050>
- [8] F. Bella, G. Griñani, J. Correa-Baena, G. Saracco, M. Gratzel, A. Hagfeldt, S. Turri, C. Gerbaldi, Improving efficiency and stability of perovskite solar cells with photocurable fluoropolymers, *Science* 354 (2016) 203–206. <https://doi.org/10.1126/science.aah4046>.
- [9] J. Wu, Z. Lan, J. Lin, M. Huang, Y. Huang, L. Fan, G. Luo, Y. Lin, Y. Xie, Y. Wei, Counter electrodes in dye-sensitized solar cells, *Chem. Soc. Rev.* 46 (2017) 5975–6023. <https://doi.org/10.1039/c6cs00752j>.
- [10] J. H. Noh, S. H. Im, J. H. Heo, T. N. Mandal and S. I. Seok, Chemical Management for Colorful, Efficient, and Stable Inorganic–Organic Hybrid Nanostructured Solar Cells, *Nano Lett.*, 2013, 13, 1764–1769. <https://doi.org/10.1021/nl400349b>.
- [11] J.P. Correa-Baena, M. Anaya, G. Lozano, W. Tress, K. Domanski, M. Saliba, T. Matsui, T.J. Jacobsson, M.E. Calvo, A. Abate, Unbroken Perovskite: Interplay of Morphology, Electro-optical Properties, and Ionic Movement, *Adv. Mater.* 28 (2016) 5031-5037. <https://doi.org/10.1002/adma.201600624>.
- [14] X. Liu, J. Wu, Y. Yang, T. Wu, Q. Guo, Pyridine solvent engineering for high quality anion-cation-mixed hybrid and high performance of perovskite solar cells, *Journal of Power Sources* 399, (2018) 144-150.
- [15] X. Li, D. Bi, C. Yi, J.-D. Decoppet, J. Luo, S.M. Zakeeruddin, A. Hagfeldt, M. Gratzel, A vacuum flash-assisted solution process for high-efficiency large-area perovskite solar cells, *Science* 353 (2016) 58-62. <https://doi.org/10.1126/science.aaf8060>.
- [16] J.-W. Lee, H.-S. Kim, N.-G. Park, Lewis Acid–Base Adduct Approach for High Efficiency Perovskite Solar Cells, *Accounts Chem. Res.* 49 (2016) 311-319. <https://doi.org/10.1021/acs.accounts.5b00440>.
- [17] T. Todorov, O. Gunawan, S. Guha, A road towards 25% efficiency and beyond: perovskite tandem solar cells, *Mol. Syst. Des. Eng.* 1 (4) (2016) 370-376. <https://doi.org/10.1039/C6ME00041J>.

[18] M. Grätzel, The light and shade of perovskite solar cells, *Nature Materials* volume13, 838–842 (2014) <https://doi.org/10.1038/nmat4065>.

[19] Idris K. Popoola Mohammed A. Gondal Talal F. Qahtan, Recent progress inflexible perovskite solar cells: Materials, mechanical tolerance and stability. *Renewable and Sustainable Energy Reviews*. <https://doi.org/10.1016/j.rser.2017.10.028>.

[20] S.S. Shin, W.S Yang, J.H. Noh, J.H. Suk, N. J. Jeon, J.H Park, High-performance flexible perovskite solar cells exploiting  $Zn_2SnO_4$  prepared in solution below 100 °C. *Nat Commun*. 6 (2015) 1–8. <http://dx.doi.org/10.1038/ncomms8410>.

[21] M. Ye, X. Hong, X. Y Liu, Recent Advancements in Perovskite Solar Cells: Flexibility, Stability and Large Scale. *J Mater Chem A* 4 (2016) 6755–71. <http://dx.doi.org/10.1039/C5TA09661H>.

[22] A. Mei, X. Li, L. Liu, Z. Ku, T. Liu, Y. Rong, M. Xu, M. Hu, J. Chen, Y. Yang, H. Han, A hole-conductor-free, fully printable mesoscopic perovskite solar cell with high stability, 345 (2014) 295. <https://doi.org/10.1126/science.1254763>.

[23] N.J. Jeon, J.H. Noh, W.S. Yang, Y.C. Kim, S. Ryu, J. Seo, S.I. Seok, Compositional engineering of perovskite materials for high-performance solar cells, *Nature* 517 (2015) 476-480. <https://doi.org/10.1038/nature14133>.

[24] J. Burschka, N. Pellet, S. Moon, R. Humphry-Baker, P. Gao, M. Nazeeruddin, M. Gratzel, Compositional engineering of perovskite materials for high-performance solar cells, *Nature* 499 (2013) 316. <https://doi.org/10.1038/nature14133>.

[25] Z. Xiao, C. Bi, Y. Shao, Q. Dong, Q. Wang, Y. Yuan, C. Wang, Y. Gao, J. Huang, Efficient, high yield perovskite photovoltaic devices grown by interdiffusion of solution-processed precursor stacking layers, *Energy Environ. Sci*. 8 (2014) 2619-2623. <https://doi.org/10.1039/C4EE01138D>.

[26] Z. Xiao, Q. Dong, C. Bi, Y. Shao, Y. Yuan, J. Huang, Solvent Annealing of Perovskite-Induced Crystal Growth for Photovoltaic-Device Efficiency Enhancement, *Adv. Mater*. 26 (2014) 6503-6509. <https://doi.org/10.1002/adma.201401685>.

[27] N. Jeon, J. Noh, Y. Kim, W. Yang, S. Ryu, S. Seol, Solvent engineering for high-performance inorganic-organic hybrid perovskite solar cells, *Nat. Mater*. 13 (2014) 897. <https://doi.org/10.1038/nmat4014>.

- [28] D. Liu, T.L. Kelly, Perovskite solar cells with a planar heterojunction structure prepared using room-temperature solution processing techniques, *Nat. Photonics* 8 (2014) 133-138. <https://doi.org/10.1038/nphoton.2013.342>.
- [29] M. Liu, M.B. Johnston, H.J. Snaith, Efficient planar heterojunction perovskite solar cells by vapour deposition. *Nature* 501 (2013) 395-398. <https://doi.org/10.1038/nature12509>.
- [30] Y. Jeon, S. Lee, R. Kang, J. Kim, J. Yeo, S. Lee, S. Kim, J. Yun, D. Kim, Planar heterojunction perovskite solar cells with superior reproducibility. *Sci. Rep.* 4 (2014) 6953. <https://doi.org/10.1038/srep06953>.
- [31] M. Liu, M. Johnston, H. Snaith, Efficient planar heterojunction perovskite solar cells by vapour deposition, *Nature* 501 (2013) 395. <https://doi.org/10.1038/nature12509>.
- [32] A. Kojima, K. Teshima, Y. Shirai, T. Miyasaka, Organometal halide perovskites as visible light sensitizers for photovoltaic cells, *J. Am. Chem. Soc.* 131 (2009) 6050-6051. <https://doi.org/10.1021/ja809598r>.
- [33] J.Y. Jeng, Y.F. Chiang, M.H. Lee, S.R. Peng, T.-F. Guo, P. Chen, T.-C. Wen,  $\text{CH}_3\text{NH}_3\text{PbI}_3$  perovskite/fullerene planar-heterojunction hybrid solar cells, *Adv. Mater.* 25 (2013) 3727-3732. <https://doi.org/10.1002/adma.201301327>.
- [34] M.Z. Liu, M.B. Johnston, H.J. Snaith, Efficient planar heterojunction perovskite solar cells by vapour deposition, *Nature* 501 (2013) 395-398. <https://doi.org/10.1038/nature12509>.
- [35] M. Xiao, F. Huang, W.C. Huang, Y. Dkhissi, Y. Zhu, J. Etheridge, A. Gray-Weale, U. Bach, Y.B. Cheng, L. Spicca, A fast deposition-crystallization procedure for highly efficient lead iodide perovskite thin-film solar cells. A fast deposition-crystallization procedure for highly efficient lead iodide perovskite thin-film solar cells, *Angew. Chem. Int. Ed.* 126 (2014) 10056-10061. <https://doi.org/10.1002/anie.201405334>.
- [36] M. Saliba, T. Matsui, J. Seo, K. Domanski, J. Correa-Baena, M. Nazeeruddin, S. Zakeeruddin, W. Tress, A. Abate, A. Hagfeldt, Cesium-containing triple cation perovskite solar cells: improved stability, reproducibility and high efficiency. *Energy Environ. Sci.* 9 (2016) 1989. <https://doi.org/10.1039/C5EE03874J>.
- [37] M. Saliba, T. Matsui, K. Domanski, J. Seo, A. Ummadisingu, S. Zakeeruddin, J. Correa-Baena, W. Tress, A. Abate, A. Hagfeldt, Incorporation of rubidium cations into

perovskite solar cells improves photovoltaic performance. *Science* 354 (2016) 206. <https://doi.org/10.1126/science.aah5557>.

[38] T. Wu, J. Wu, Y. Tu, X. He, Z. Lan, M. Huang, J. Lin, J. Solvent engineering for high-quality perovskite solar cell with an efficiency approaching 20%. *Power Sources* 365 (2017) 1–6. <https://doi.org/10.1016/j.jpowsour.2017.08.074>.

[39] A. Abate, J. Correa-Baena, M. Saliba, M. Su'ait, F. Bella, Frontispiece: Perovskite Solar Cells: From the Laboratory to the Assembly Line, *Chem. Eur J.* 24 (2018) 3083–3100. <https://doi.org/10.1002/chem.201704507>.

[40] H. Choi, J. Jeong, H. Kim, S. Kim, B. Walker, G. Kim, J. Kim, Cesium-doped methylammonium lead iodide perovskite light absorber for hybrid solar cells *Nano Energy* 7 (2014) 80. <https://doi.org/10.1016/j.nanoen.2014.04.017>.

[41] J. Lee, D. Kim, H. Kim, S. Seo, S. Cho, N. Park, Formamidinium and cesium hybridization for photo-and moisture-stable perovskite solar cell *Adv. Energy Mater* 5 (2015) 201501310. <https://doi.org/10.1002/aenm.201501310>.

[42] J. Burschka, N. Pellet, S. Moon, R. Humphry-Baker, P. Gao, M. Nazeeruddin, M. Gratzel, Sequential deposition as a route to high-performance perovskite-sensitized solar cells, *Nature*, 499 (2013) 316. <https://doi.org/10.1038/nature12340>.

[43] J. Liang, Z. Liu, L. Qiu, Z. Hawash, L. Meng, Z. Wu, Y. Jiang, L.K. Ono, Y. Qi, Enhancing Optical, electronic, crystalline, and morphological properties of cesium lead halide by Mn substitution for high-stability all-inorganic perovskite solar cells with carbon electrodes, *Adv. Energy Mater.* 8 (2018) 1800504.

[44] C.F.J. Lau, X. Deng, J. Zheng, J. Kim, Z. Zhang, M. Zhang, J. Bing, B. Wilkinson, L. Hu, R. Patterson, S. Huang, A. Ho-Baillie, Enhanced performance via partial lead replacement with calcium for a CsPbI<sub>3</sub> perovskite solar cell exceeding 13% power conversion efficiency, *J. Mater. Chem. A* 6 (2018) 5580–5586

[45] G. Kieslich, S. Sun, K. Cheetham, Solid-state principles applied to organic–inorganic perovskites: new tricks for an old dog, *Chem. Sci.*, 2014, 5, 4712. <https://doi.org/10.1039/C4SC02211D>.

[46] O. J. Weber, K. L. Marshall, L. M. Dyson, M. T. Weller. Structural diversity in hybrid organic–inorganic lead iodide materials *Acta Cryst.* (2015) B71, 668–678. <https://doi.org/10.1107/S2052520615019885>.

- [47] H. Lin, C. Zhou, Y. Tian, T. Siegrist, T. B. Ma, Low-Dimensional Organometal Halide Perovskites. *Energy Lett.* 2018, 3, 54–62. <https://doi.org/10.1021/acsenergylett.7b00926>.
- [48] Q. Wang, F. Lina, Chu-Chen C, T. Zhaoa, M. Eslamian, A. K.Y. Jen, Enhancing efficiency of perovskite solar cells by reducing defects through imidazolium cation incorporation *Materials Today Energy*, 7, 2018, 161–168. <http://doi.org/10.1016/j.mtener.2017.09.007>.
- [49] Yi. Z., Giulia G., Zhafu F., Erfan Shirzadi., Xuehui L., Emad Oveise., Farzaneh., Rosario S., Yaqing F., Mohammad K. N., Paul.J. D. *Nano Energy* 58 (2019) 105–111].
- [50] A. Sutanto, S. Lan, C. Cheng, S. B. Mane, H-P. Wu, M. Leonardus, M-Y. Xie, S-C. Yeh, C-W. Tseng, C-T. Chen, E. W-G. Diau, C-H. Hung, *Solar Energy Materials and Solar Cells* 172 (2017) 270–276. <https://doi.org/10.1016/j.solmat.2017.07.043>.
- [51] C. C. Stoumpos, C. D. Malliakas, M. G. Kanatzidis, Semiconducting Tin and Lead Iodide Perovskites with Organic Cations: Phase Transitions, High Mobilities, and Near-Infrared Photoluminescent Properties *Inorg. Chem.* 52 (2013) 9019–9038. <https://doi.org/10.1021/ic401215x>.
- [52] N. Pellet, P. Gao, G. Gregori, T. Y. Yang, M. K. Nazeeruddin, J. Maier, M. Grätzel, Mixed-organic-cation perovskite photovoltaics for enhanced solar-light harvesting. *Angew. Chem. Int. Ed.* 53 (2014) 3151–3157. <https://doi.org/10.1002/anie.201309361>.
- [53] Y. Huang, L. Li, Z. Liu, H. Jiao, Y. He, X. Wang, R. Zhu, D. Wang, J. Sun, Q. Chen, H. Zhou, J. The intrinsic properties of  $\text{FA}_{(1-x)}\text{MA}_x\text{PbI}_3$  perovskite single crystals, *Mater. Chem. A* 5 (2017) 8537–8544. <https://doi.org/10.1039/C7TA01441D>.
- [54] R. Yinhke, D. Bin D, X. Yafeng, H. Yang, L. Zhaoquian, H. Linhua, H. Tasawar, W. Hongxia, Z. Jun, D. Songyuan. *Science China Materials* 2017, 60(5): 392-398.
- [55] N. J. Jeon, J. H. Noh, Y.C. Kim, W.S. Yang, S. Ryu, S.I. Seok, Solvent engineering for high-performance inorganic-organic hybrid perovskite solar cells, *Nat. Mater.* 13 (2014) 897-903.
- [56] N. K. Noel, A. Abate, S. D. Stranks, E. S. Parrott, V. M. Burlakov, A. Goriely and H. J. Snaith, *ACS Nano*, 2014, 8, 9815–9821.

Table 1. IR absorption bands ( $\text{cm}^{-1}$ ) and their assignments for the synthesized compounds.

Hybrid system	$\nu$ N-H st	$\nu$ C- H st	$\nu$ C-Nst	$\nu$ C=Cst	$\nu$ C-H oop	$\nu$ C-H ring
<b>ImI-PbI<sub>2</sub> -1:1</b>	3263	3121	1428	1621	1030	735
<b>ImI-PbI<sub>2</sub> -2:1</b>	3476	3121	1397	1633	1030	746

## **Declaration of interest statement**

The authors declare there is no conflict of interests

Journal Pre-proof